Solar Physics (2023) 298:86
https://doi.org/10.1007/s11207-023-02177-8

RESEARCH

Analysis of the Solar Flare Index for Solar Cycles 18 – 24: Extremely Deep Gnevyshev Gap in the Chromosphere

Jouni Takalo[1]

Received: 27 March 2023 / Accepted: 6 June 2023 / Published online: 7 July 2023

Abstract
We study the solar flare index (SFI) for the Solar Cycles 18 – 24. We find that SFI has deeper Gnevyshev gap (GG) in its first principal component than other atmospheric parameters. The GG is extremely clear especially in the even cycles.

The GG of the SFI appears about a half year later as a drop in the interplanetary magnetic field near the Earth and in the geomagnetic Ap-index. The instantaneous response of the magnetic field to solar flares, however, shows about two to three days after the eruption as a high, sharp peak in the cross-correlation of the SFI and Ap-index and as a lower peak in SFI vs. IMF B cross-correlation. We confirm these rapid responses using superposed-epoch analysis.

The most active flare cycles during 1944 – 2020 are Cycles 19 and 21. Cycle 18 has very strong SFI days as many as Cycle 22, but it has the least nonzero SFI days in the whole interval. Interestingly, Cycle 20 can be compared to Cycles 23 and 24 in its low flare activity, although it is located between the most active SFI cycles.

Keywords Solar flare · Solar cycles · SFI · Ap-index · IMF · Cross-correlation · PCA · T-test

1. Introduction

Solar flare is a burst of radiation coming from the release of magnetic energy associated with sunspots. Flares are the most energetic phenomena in the Sun. They are seen as bright areas on the Sun and can last from minutes to hours. The primary ways to monitor flares are in X-rays, energetic particles, and optical light. Kleczek (1952) quantified solar flares through a formula $Q =$ Importance $\times$ time to be able approximate the daily flare activity. This quantity, which is defined in more detail in the Data and Methods section, is called the Solar Flare Index (SFI).

The earliest studies of Solar Flare Index (SFI) are based on the recordings of the Astronomical Institute Ondřejov Observatory of the Czech Academy of Sciences. Švestka (1956) studied the flares of Cycles 17 and 18 based on this database. Knoška and Petrašek (1984)

✉ J. Takalo
jouni.j.takalo@oulu.fi; jojuta@gmail.com

[1] Space Physics and Astronomy Research Unit, University of Oulu, POB 3000, FIN-90014, Oulu, Finland

studied the flare activity of Cycle 20, and Knoska (1985) studied the annual distribution of the flares for the interval 1937 – 1976 and compared those with the variation of sunspot numbers of the same interval. Most of the studies of SFI have, however, concentrated on spectral studies of the index for Cycles 20 – 24 (Özgüç and Ataç, 1989; Özgüç, Ataç, and Rybák, 2003; Ataç and Özgüç, 2006; Mendoza and Velasco-Herrera, 2011; Özgüç et al., 2021). Mendoza and Velasco-Herrera (2011) studied also SFI power in the midterm periodicities (1–2 years) for Cycles 20 – 23 and concluded that the flare index is diminished during the low-activity Cycle 20. The power increases during Cycles 21 and 22, but Cycle 23 shows again weaker power than Cycles 21 and 22.

Velasco Herrera et al. (2022) reconstructed the solar flare index (SFI) to study the solar chromospheric variability from 1937 to 2020. The new SFI database is a composite record of the Astronomical Institute Ondřejov Observatory of the Czech Academy of Sciences from 1937 – 1976 and the records of the Kandilli Observatory of Istanbul, Turkey, from 1977 – 2020. They studied the periodicities of the flare cycles using wavelet transform. They also found using the method called power anomaly that the most active flare cycles were Cycles 17 (incomplete cycle), 19, and 21, whereas Cycles 20, 22, 23, and 24 were the weakest ones with Cycle 18 being intermediate in flare activity. Especially, Cycle 20 is much weaker in flare index than in sunspot numbers.

Gnevyshev first noticed that a solar cycle has usually twofold maximum, i.e., two maxima with a gap, nowadays called Gnevyshev gap (GG), in between (Gnevyshev, 1963, 1977; Schove, 1979). Gnevyshev (1967) states that each 11-year cycle of solar activity consists of two processes with different physical properties. The variety of shapes of the 11-year curves depends on the way these processes overlap. All events in the photosphere, chromosphere and corona, and all kinds of emissions like the radio- and corpuscular emissions take part in these two processes.

It is nowadays clear that a solar cycle has three phases, an ascending phase, a descending phase, and between them Gnevyshev gap (GG) (Storini et al., 2003; Ahluwalia and Kamide, 2004; Bazilevskaya, Makhmutov, and Sladkova, 2006; Norton and Gallagher, 2010; Du, 2015), which is a kind of separatrix between the first two (main) phases. The time of the Gnevyshev gap is 45–55 months after the start of the nominal cycle, that is, approximately 33–42% into the cycle after its start (Takalo and Mursula, 2018; Takalo, 2020b).

Storini et al. (2003) gave a review of the earlier studies of the GG effects in different space-weather parameters. They state that the GG provides a significant time interval in which a relative quietness in the solar terrestrial system ensures no dangerous phenomena in the Earth's environment. Hence GG is relevant for the space weather, and signatures of the GG are present in most of the terrestrial physical parameters.

We study here the SFI using principal component analysis and show that SFI has a clear Gnevyshev gap (GG) in its first principal component. This gap is deeper than in other solar indices and is especially clear in the even cycles. We study the mutual strength of the SFI cycles and the cross-correlation of the geomagnetic disturbance index Ap with SFI. This paper is organized as follows. In Section 2, we present the data and methods used in this study. In Section 3, we compare the first principal components of selected solar atmospheric indices and present histograms of different categories of SFI days in Section 4. Section 5 deals with the correlation of SFI and geomagnetic disturbances as measured with Ap-index. In Section 6, we compare the mutual strengths of SFI cycles and give our conclusions in Section 7.

Table 1 Sunspot-cycle lengths and dates [fractional years, and year and month] of (starting) sunspot minima for Solar Cycles 18 – 24.

Sunspot cycle number	Fractional year of minimum	Year and month of minimum	Cycle length [years]
18	1944.1	1944 February	10.2
19	1954.3	1954 April	10.5
20	1964.8	1964 October	11.7
21	1976.5	1976 June	10.2
22	1986.7	1986 September	10.1
23	1996.8	1996 October	12.2
24	2009.0	2008 December	11.0
25	2020	2019 December	

2. Data and Methods

2.1. Solar Flare Index (SFI)

The solar flare index used in this study was recently published by Velasco Herrera et al. (2022). This database is a composite record of the Astronomical Institute Ondřejov Observatory of the Czech Academy of Sciences from 1937 – 1976 and the records of the Kandilli Observatory of Istanbul, Turkey, from 1977 – 2020. Although the exact total energy of the solar flare event is impossible to determine, the daily and monthly databases are calculated using Hα-related white-light flares through the formula (Kleczek, 1952; Knoška and Petrašek, 1984; Özgüç and Ataç, 1989)

$$Q = I \times t, \tag{1}$$

where I is the importance of the flare, and t is the duration of the flare in minutes. The importance consists of two factors, the area of the flare (S, 1, 2, 3, 4) and the brilliance of the flare: F(aint), N(ormal), anf B(right) (Özgüç, Ataç, and Rybák, 2002). The lengths of the solar cycles used in this study are shown in Table 1.

2.2. Principal Component Analysis Method

Principal component analysis is a useful tool in many fields of science including chemometrics (Bro and Smilde, 2014), data compression (Kumar, Rai, and Kumar, 2008), and information extraction (Hannachi, Jolliffe, and Stephenson, 2007). PCA finds combinations of variables that describe major trends in the data. PCA has earlier been applied, e.g., to studies of the geomagnetic field (Bhattacharyya and Okpala, 2015), geomagnetic activity (Holappa, Mursula, and Asikainen, 2014; Takalo, 2021b), ionosphere (Lin, 2012), the solar background magnetic field (Zharkova et al., 2015), variability of the daily cosmic-ray count rates (Okpala and Okeke, 2014), solar corona (Takalo, 2022b), and for separation of the cosmic-rays to Schwabe and Hale cycle related components (Takalo, 2022a).

In this paper, we compare, using PCA, the solar flare index (SFI) to sunspot numbers (SSN2), solar plage areas (PA), solar 10.7 cm radio flux (RF), and coronal index of solar activity (CI) for Solar Cycles 18 – 24. (We omit Cycle 17, because its SFI data is incomplete.) To this end, we estimate that the average length of the cycle is 130 months and use it as a representative solar cycle. We first resample the monthly data such that all cycles

have the same length of 130 time steps (months), i.e., about the average length of the Solar Cycles 18 – 24 (Takalo and Mursula, 2018; Takalo, 2021b). This effectively elongates or abridges the cycles to the same length. Before applying the PCA method to the resampled cycles, we standardize each individual cycle to have zero mean and unit standard deviation. This guarantees that all cycles have the same weight in the study of their common shape. Standardized data are then collected into the columns of the matrix X, which can be decomposed as (Hannachi, Jolliffe, and Stephenson, 2007; Holappa et al., 2014; Takalo and Mursula, 2018)

$$X = U\ D\ V^T\ , \tag{2}$$

where U and V are orthogonal matrices, V^T is the transpose of a matrix V, and D is the diagonal matrix $D = diag\,(\lambda_1, \lambda_2, \ldots, \lambda_n)$ with λ_i the ith singular value of the matrix X. The principal components are obtained as the column vectors of

$$P = UD. \tag{3}$$

The column vectors of the matrix V are called empirical orthogonal functions (EOF), and they represent the weights of each principal component in the decomposition of the original normalized data of each cycle X_i, which can be approximated as

$$X_i = \sum_{j=1}^{N} P_{ij}\, V_{ij}\ , \tag{4}$$

where j denotes the jth principal component (PC). The explained variance of each PC is proportional to square of the corresponding singular value λ_i. Hence the ith PC explains a percentage

$$\frac{\lambda_i^2}{\sum_{k=1}^{n}\lambda_k^2} \cdot\ 100\% \tag{5}$$

of the variance in the data. In this study, we use only the first principal component (PC1), which tells the main features of the data and is practically the average of the original data set.

2.3. Two-Sample T-Test

The two-sample T-test for equal mean values is defined as follows. The null hypothesis assumes that the means of the samples are equal, i.e., $\mu_1 = \mu_2$. The alternative hypothesis is that $\mu_1 \neq \mu_2$. The test statistic is calculated as

$$T = \frac{\mu_1 - \mu_2}{\sqrt{s_1^2/N_1 + s_2^2/N_2}}, \tag{6}$$

where N_1 and N_2 are the sample sizes, μ_1 and μ_1 are the sample means, and s_1^2 and s_2^2 are the sample variances. If the sample variances are assumed equal, then the formula reduces to

$$T = \frac{\mu_1 - \mu_2}{s_p\sqrt{1/N_1 + 1/N_2}}, \tag{7}$$

where

$$s_p^2 = \frac{(N_1 - 1)s_1^2 + (N_2 - 1)s_2^2}{N_1 + N_2 - 2}. \tag{8}$$

The rejection limit for the two-sided T-test is $|T| > t_{1-\alpha/2,\nu}$, where α is the significance level, and ν denotes degrees of freedom. The values of $t_{1-\alpha/2,\nu}$ are published in T-distribution tables (Snedecor and Cochran, 1989; Krishnamoorthy, 2006; Derrick, Deirdre, and White, 2016). Now if $p < \alpha = 0.05$, then the significance is at least 95%, and if $p < \alpha = 0.01$, then the significance is at least 99%.

2.4. Cross-Correlation

The cross-correlation function measures similarity between a time series and lagged versions of another time series as a function of the lag. Let us consider two time series (vectors) x_t and y_t. We define the cross-covariance as (Box et al., 2016)

$$c_{xy}(k) = \frac{1}{T}\sum_{t=1}^{T-k}(x_t - \overline{x})(y_{t+k} - \overline{y}), k = 0, 1, 2, \ldots, \tag{9}$$

and

$$c_{xy}(k) = \frac{1}{T}\sum_{t=1}^{T+k}(y_t - \overline{y})(x_{t-k} - \overline{x}), k = 0, -1, -2, \ldots, \tag{10}$$

where $\overline{x}$ and $\overline{y}$ are the sample means of the time series. If we use only part of the series in calculation, then we call the procedure sample cross-covariance. The sample standard deviations are $s_x = \sqrt{c_{xx}(0)}$ and $s_x = \sqrt{c_{yy}(0)}$. As an estimate of the sample cross-correlation, we have

$$r_{xy}(k) = \frac{c_{xy}(k)}{s_x s_y}, k = 0, \pm 1, \pm 2, \ldots . \tag{11}$$

We calculate here the cross-correlation of two time series in two ways, i.e., from a limited sample of the time series and using circular cross-correlation of the time series through the whole solar cycle. The fastest way to do the process is by using the Fourier transforms of the vectors **x**, **y**, multiplying them (no conjugate is needed here, because the vectors are real valued), and taking the inverse Fourier transform of the product. The result can be normalized by dividing by the norms of the vectors.

3. PC Analysis of Selected Solar Atmospheric Indices

Principal component analysis (PCA) is a good method to distinguish essential features in the time series. This method is especially good for analysis of time series that depend on a single strong period, e.g., the solar cycle. This is because it is probable that this period forms the base of the first principal component (PC1). Because PCs are orthogonal, the second component is most likely related to the period, which is half of the solar period. Now if the PC2s of the successive cycles are in opposite phase, then we get twice the original period, i.e., the Hale period, at least in the case the time series in question is also depending on the

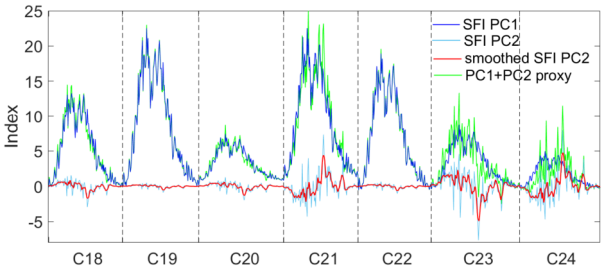

Figure 1 The PC1, PC2, smoothed PC2, and the PC1 + PC2 time series of the solar flare index (SFI) for Solar Cycles 18 – 24.

Hale cycle. (Notice that the normalized solar cycle is actually one period of a sine wave, and we know that $\sin(k\alpha)$ and $\sin(n\alpha)$ are orthogonal when $k \neq n$.) In this way, PCA is better here than, e.g., Independent Component Analysis (ICA), which finds components that are maximally independent from each other, e.g., noise from the signal (ICA components are not necessarily orthogonal). Takalo (2021b, 2022a) has actually shown, using PCA, that the aa-index and cosmic-ray indices can be separated into components related to the Schwabe and Hale cycles.

Here we are interested mostly in the PC1 of SFI and compare it to other PC1s of solar cycle-related indices. Because the GG is known as an essential feature of the solar cycle, it is also usually present in the PC1, which is the component accounting for the most variance of the data. That is why we conducted PCA for several solar indices. Because PCA is a matrix-based method, we use the procedure described earlier to have all Cycles 18 – 24 the same length 130 time steps (months), which is about the average length of those cycles. The idea in this method is that we suppose all cycles to have the same dynamical phases, except that cycles differ in the duration of the phases. The separate Cycles 18 – 24 form the columns of the matrix X in Equations 2–4. The first and second principal components of each cycle i are X_i s with $j = 1$ and $j = 2$, respectively in Equation 4. We then return each cycle back to its original length and then back to its original amplitude by multiplying PCs of each cycle by the standard deviation of the original cycle and adding the mean value of the original cycle to PC1. Now we can construct full PC1 and PC2 time series by concatenating the cycles to their original order. Figure 1 shows the time series PC1 and PC2 series and their sum time series PC1 + PC2 of the SFI for Solar Cycles 18 – 24. Note that every cycle has evidently the same gap in their same PC1. Some cycles have, however, very large fluctuations in their PC2, which explains 12.4% of the variance in the solar cycle time series. This is the case especially for Cycles 21, 23, and 24. For Cycle 23, the PC2 lowers the GG but makes it still deeper for Cycle 21 and 24. Note that there exists PC3 that accounts for 8.2% of the variance (not shown here) and is especially large for Cycles 20 and 23. Other PCs are quite negligible.

Figures 2a,b show the power spectra of the PC1 and PC2 time series for the Solar Cycles 18 – 24, respectively. We have low-pass filtered the time series, because we are interested here only in multiple year periods in the data. The dashed red lines are 99% significance levels of the red-noise data. Red-noise is calculated as a power spectrum from the time series

$$x_n = \alpha\, x_{n-1} + z_n, \tag{12}$$

where α is the lag-1 autocorrelation, and z_n is a Gaussian white noise. Furthermore, we adjust the length and variance of the red-noise time series to those of the original PC1 or PC2 time series (Torrence and Compo, 1998; Mendoza and Velasco-Herrera, 2011; Oloketuyi,

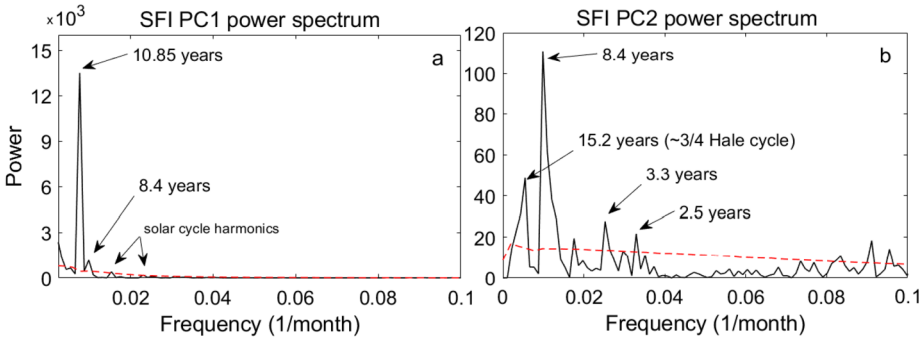

Figure 2 a) The power spectrum of SFI PC1 time series for SC18 – SC24. b) The power spectrum of SFI PC2 time series for SC18 – SC24.

Liu, and Zhao, 2019). There are other ways to approximate the significance level, e.g., the so-called false alarm probability (FAP) method (Özgüç, Ataç, and Rybák, 2003). We, however, think that it is not the best way in our case to find the confidence limit. This is because we have separated different periods into several different orthogonal time series. Note that most of the earlier studies have concentrated on the short- and mid-term periods in the solar flares as discussed in the Introduction. It is understandable that by far the strongest power in PC1 is at 10.85 years (130 months), which is the average length of Solar Cycles 18 – 24. Another peak above the red-noise level in the PC1 time series is the 8.4-year period. The rest of the peaks are negligible, and the two peaks marked in Figure 2a are periodic peaks of the solar cycle. It is interesting that the 8.4-year peak is also present and is in fact the most powerful peak in the power spectrum of the PC2 time series (Figure 2b). The other peaks above the 99% confidence level are about 15.2-, 3.3-, and 2.5-year periods. Note that the PC2 power spectrum does not show the solar cycle period. Because the resolution for the power spectrum of quite short time series (monthly data) is quite poor, we suppose that the periods 3.3 and 8.4 added together make the solar cycle (note that these peaks are skewed to the right, which means that the exact period is somewhat less than the aforementioned values). On the contrary, the 15.2-year peak is skewed to the left and should probably be a slightly longer period. We believe that this peak is 3/4 of the magnetic 22-year Hale cycle. Velasco Herrera et al. (2022) and Özgüç et al. (2021) reported in their research about 3.5-year and 3.2-year peaks, respectively. These are quite near to our 3.3-year period in PC2 power spectrum. Note that we get 3.16- and 1.46-year peaks for the power spectrum of the PC3 time series (not shown here). These peaks may be related to the 1153-day peak in total solar surface and about 540-day peak in the northern and southern hemispheres of the Sun reported by Özgüç, Ataç, and Rybák (2003).

Figures 3a,b show the first principal components (PC1) for four solar atmospheric indices for Cycles 18 – 24, i.e., for the sunspot number SSN2 (photosphere), solar flare index (SFI) (chromosphere), plage area (PA) (chromosphere), 10.7-cm radio flux (RF) (high chromosphere, low corona), and solar green line corona index (CI), which is actually measured at low altitude (about 60 arcsecs) above the surface of the Sun. It is surprising that SFI has the most conspicuous gap between 46 to 53 (shown as vertical dashed lines) months in its PC1. Although PC1 for SFI explains just 62.7% of the total variance of the data, it is, as said earlier, practically the average of Cycles 18 – 24. This is seen in Figure 4a, which shows the PC1 reverted back to original amplitude and the average of Cycles 18 – 24. Note that the gap, which we believe is the Gnevyshev gap, has a two-fold minimum with a peak between.

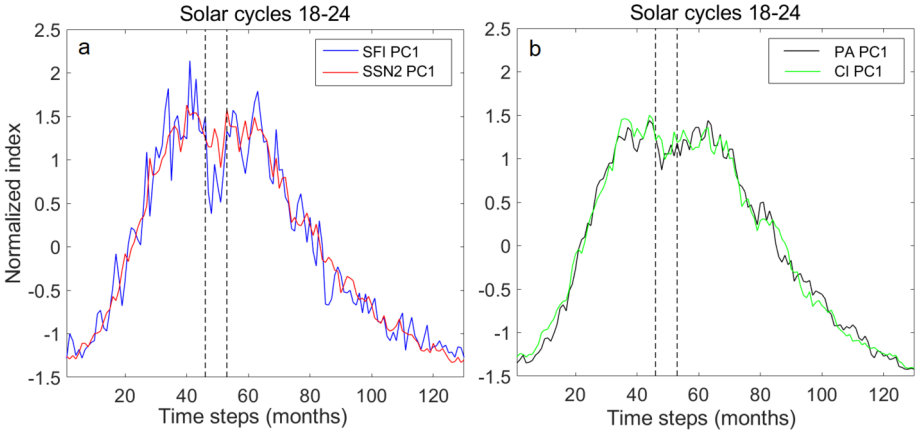

Figure 3 a) The PC1s of solar flare index (SFI) and sunspot numbers (SSN2). b) The PC1s of plage area (PA) index and solar corona index (CI).

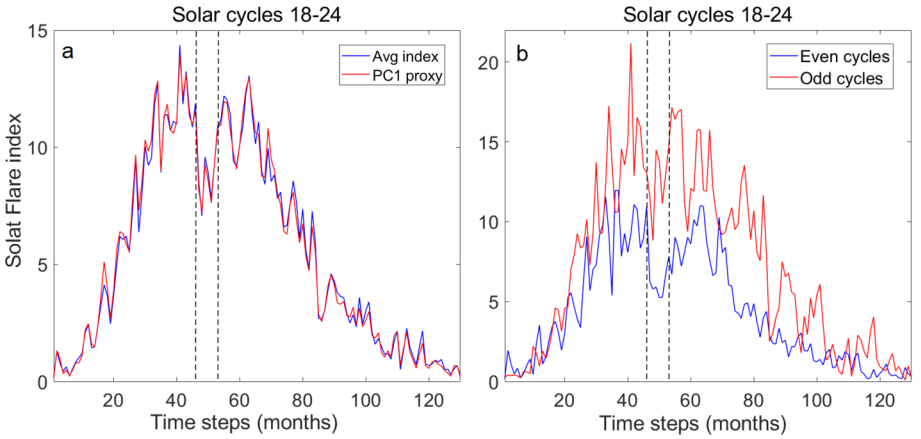

Figure 4 a) The PC1 and average cycle of SFI for Cycles 18 – 24. b) The average cycle for even and odd Cycles 18 – 24.

The bottom of the first minimum at 48 months is 40% smaller than the peak two months earlier. It turns out that the first minimum is due to both even and odd cycles, and the second minimum mainly to even cycles (see Figure 4b). Note also that the drop for the even cycles is about 50%.

To study the GG in more detail, we use the daily data of the aforementioned indices. We have interpolated all cycles to have 3945 days, which is about the average number of days in Cycles 18 – 24. Figures 5a,b show the total amounts of SFI, SSN2, PA and SFI, CI, RF for even Cycles 18 – 24, respectively. Note that SSN2 has been adjusted to enable the presentation of the indices on the same scale. Furthermore, all indices are smoothed over 31 or 61 days (depending how spiky they are in order to make the figure more readable). Note that the GG locates similarly for SFI, SSN2, and PA in Figure 5a, but SFI has by far the deepest decline between the dashed vertical lines, which are 1380 and 1660 days after the minimum of the cycles, i.e., show about a nine-month window. The SFI and RF are

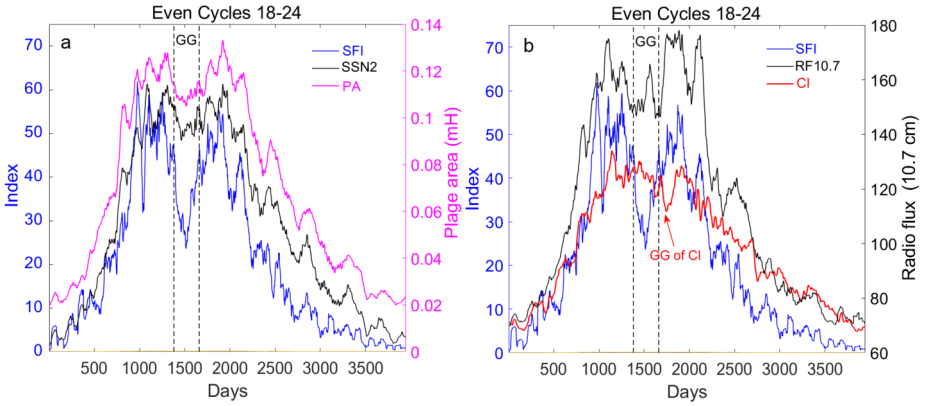

Figure 5 a) The total daily index of SFI, SSN2, and PA for even Cycles 18 – 24. b) The total daily index of SFI, CI, and RF for even Cycles 18 – 24. (The indices are smoothed over 31 days or 61 days, and SSN2 is adjusted to enable presenting on the same scale as other indices.)

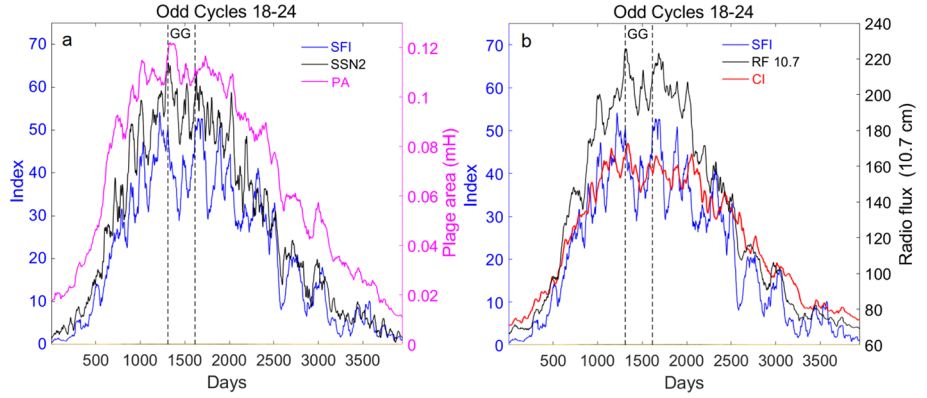

Figure 6 a) The total daily index of SFI, SSN2, and PA for odd Cycles 18 – 24. b) The total daily index of SFI, CI, and RF for odd Cycles 18 – 24. (The indices are smoothed over 31 days or 61 days, and SSN2 is adjusted to enable presenting on the same scale as other indices.)

also simultaneous in Figure 5b, except that RF is twofold with a peak in between the GG region. The GG in the CI locates, however, later but is twofold like the GG of the RF index. Figures 6a,b show the total amounts of SFI, SSN2, PA and SFI, CI, RF for the daily odd Cycles 18 – 24. Note again that the decline of SFI for the odd cycles is not as deep as for the even cycles. The clearest difference here for the even cycles in Figure 5 is that all GGs have two minima with a peak in between. The GG window is also somewhat earlier for the odd cycles compared to the even cycles, i.e., between 1310 and 1615 days after the minimum. It also seems that the GG starts somewhat later for all other indices than the SFI for the odd cycles. Interestingly, as seen in Figure 6a the GG for SSN2 starts about one solar rotation later than the decline for the SFI. Note also from Figure 6b that the start of the decline of the RF and CI is simultaneous for the odd cycles and also about one solar rotation later than the decline for the SFI. These lags may be due to long-living recurrent sunspot groups (Nagovitsyn, Ivanov, and Osipova, 2019). On the other hand, the GG of the PA starts much

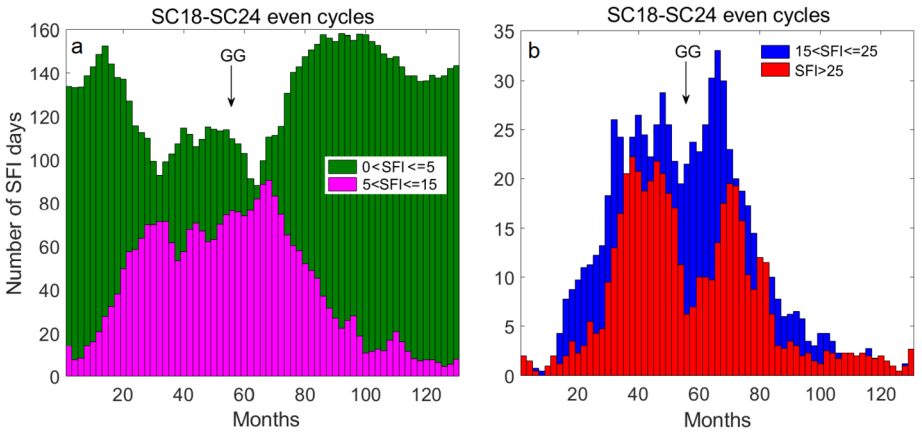

Figure 7 The histograms of amounts for SFI days a) in categories weak ($0<\text{SFI}\leq 5$) and moderate ($5<\text{SFI}\leq 15$) and b) in categories strong ($15<\text{SFI}\leq 25$) and very strong ($\text{SFI}>25$) for even Cycles 18 – 24.

later and in fact at about the time of 1380 days, marked in Figure 5 as a starting point of the GG window.

4. Histograms of Daily SFIs

The huge GG in the average cycle of SFI waked our interest in more detailed analysis of the gap. We divide the daily values of SFI to four categories: weak ($0 < \text{SFI} \leq 5$), moderate ($5 < \text{SFI} \leq 15$), strong ($15 < \text{SFI} \leq 25$), and very strong ($\text{SFI} > 25$). Figures 7 and 8 show the histograms of the categories for the even and odd Cycles 18 – 24, respectively. Each bar represents the daily values of two months. Because the SFI data are quite spiky, we smoothed the data over six months. Looking at the figures, it is evident that odd cycles have more strong and very strong category SFI days at the maximum of the cycles and, consequently, the deeper valley in the histogram of the weak category days. Note that there is a hump at the GG site in the histogram of the weak category. Both even and odd cycles have about the same amount moderate category SFI days. The even cycles seem to have deeper GG (shown with an arrow) in strong and especially very strong category days. Note that, consequently, there are more moderate and weak category days during the gap in the even cycles. On the contrary, the GG in the odd cycles exists already in the moderate category histogram and also in the strong and very strong category histograms. The difference of the odd cycles compared to even cycles is that the gap is not very deep in any of these categories. The GG is also somewhat earlier for the odd cycles than the even cycles. These results are consistent with the earlier studies by Takalo (2020a,b) concerning the GG for the sunspot numbers and sunspot groups.

5. The Response of IMF Bv2 and Ap-Index to SFI

To show the response of IMF and geomagnetic field to SFI, we reconstruct 3945-day-long data of SFI for even Cycles 18 – 24, daily Ap-data for even Cycles 18 – 24, and daily interplanetary magnetic field/solar wind function Bv^2 (Ahluwalia, 2000) for even Cycles 20, 22,

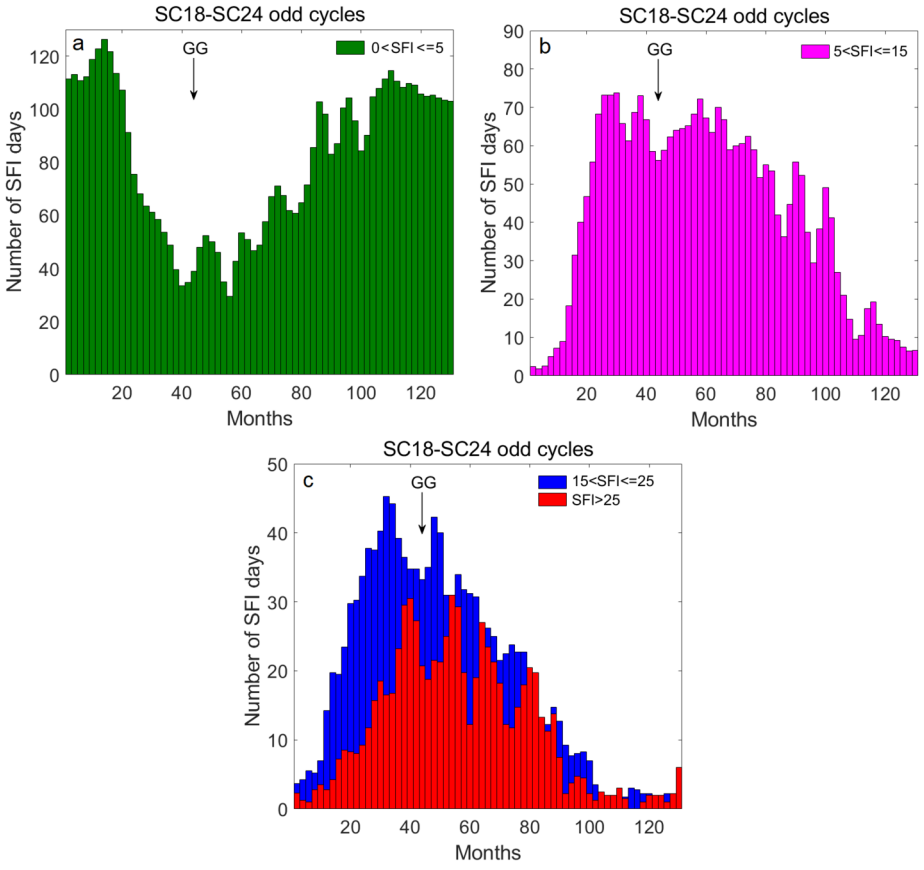

Figure 8 The histograms of amounts for SFI days a) in category weak ($0<\text{SFI}\leq 5$), b) in category moderate ($5<\text{SFI}\leq 15$), and c) in categories strong ($15<\text{SFI}\leq 25$) and very strong ($\text{SFI}>25$) for odd Cycles 18 – 24.

and 24. (Note that we have IMF data only for Cycles 20 – 24.) We use 3945 days as an average length of the cycle, because it is about 130 months, which we used earlier in the monthly analysis (see also Takalo, 2021a). Figures 9a,b,c show the sequence of daily averages of SFI, Bv^2, and Ap-index for even Cycles 18 – 24 (except 20 – 24 for Bv^2), respectively. Here the indices are smoothed using trapezoidal smoothing over 61 points (rectangular moving-average smoothing with window end points having only half of the weight of the inner points). The vertical dashed lines are at 1384, 1567, and 1725 days from the start of the cycle. The decline of the daily SFI values (Figure 9a) between lines 1384 – 1725 (mean = 6.70) is at least 99% significant in the two-sample T-test for unequal mean compared to similar intervals earlier ($p < 10^{-11}$, mean = 9.66) and after ($p < 10^{-10}$, mean = 8.96) as calculated from the unsmoothed data. Note, however, that the deepest phase of the decline between 1384 and 1567 days lasts about 6 months, which we suppose to be the main GG phenomenon. Note also a quasi-periodic structure in the average SFI. The mean period of this fluctuation is about 150 days, which has been found to be the period of various activities of the Sun (Rieger et al., 1984; Lou, 2000; Richardson and Cane, 2005; Takalo, 2021a; Li et al., 2021; Velasco Herrera et al., 2022).

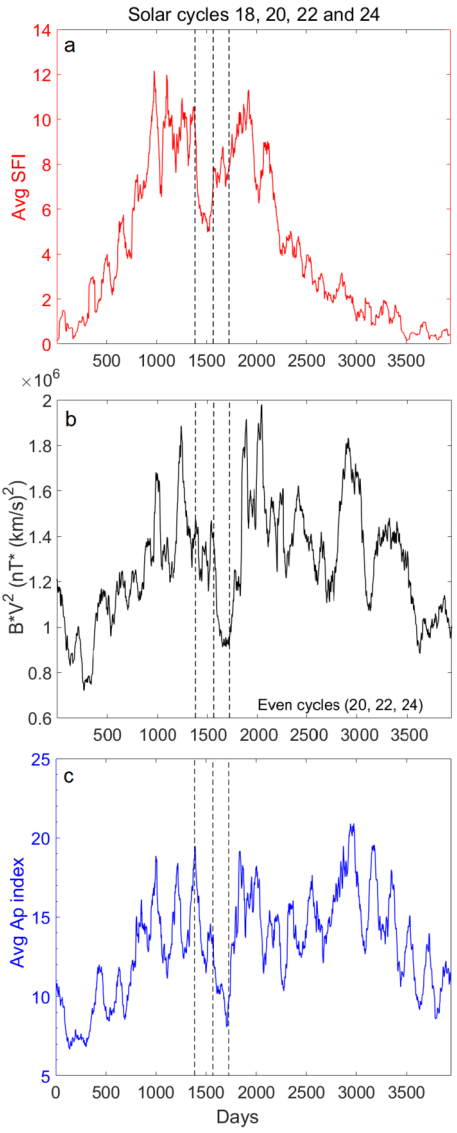

Figure 9 Top panel: The average solar flare index for even Solar Cycles 18 – 24. Middle panel: The average IMF Bv^2-component for even Solar Cycles 20 – 24. Bottom panel: The average Ap-index for even Solar Cycles 18 – 24.

The decline in IMF Bv^2 near the Earth (Figure 9b) and Ap-index (Figure 9c) is not simultaneous with the drop in the SFI. There is, however, a deep prolonged decline, which lasts at least until day 1725. Note the similar shape of the IMF Bv^2 behavior between 1567 – 1725 days compared to SFI between 1384 – 1567 days. If we assume that this part of the decline (which is also related to other solar events) travels with the speed of solar wind, then the lag is quite near to six months, i.e., about same as the lag from the drop in SFI at 1384 to drop in IMF Bv^2 and Ap at 1567 days. Note that geomagnetic disturbances (or at this case, absence of disturbances) usually lag the solar indices some months. For example, Takalo (2021b) has estimated that the aa minima for Cycles 10 – 24 lag the sunspot number minima from 3 (Cycle 14) to 17 (Cycle 16) months, i.e., 10 months on average.

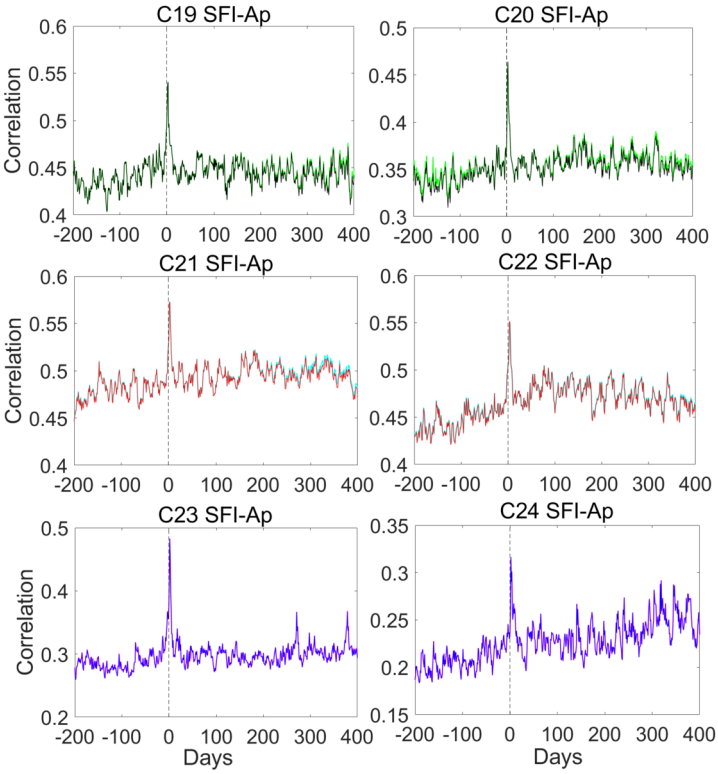

Figure 10 The cross-correlations between SFI and Ap-index for Solar Cycles 18 – 24.

Another case is the instantaneous response of the geomagnetic field to powerful events like CME/shock waves, which may have transit times measurable from tens of hours to several days (Suresh, Gopalswamy, and Shanmugaraju, 2022; Cliver et al., 2022). These events are often related to Hα flares. Figure 10 shows the cross-correlation of SFI and Ap-index for the Solar Cycles 19 – 24. Negative days are for Ap preceding the SFI and positive days Ap succeeding the SFI. There is a peak maximizing at (positive) two to three days in all cross-correlation curves. Note also that the cross-correlation stays somewhat higher after the peak. The black (uppermost panels), red (middle panels), and blue (lowest panel) are calculated as a limited interval around the zero point, and the green (uppermost panels), cyan (middle panels), and magenta (lowest panel) are calculated using the circular cross-correlation. The overall level of the cross-correlation seems to be proportional to the strength of the corresponding cycle, although not exactly. The highest peak above the overall level is for Cycle 23, which may be due to some strong flares at the beginning of the new millennium. Figure 11 shows the magnifications of Figure 10 with two standard deviations as a lilac color. Note that the standard deviation is narrowest for the aforementioned Cycle 23.

Another way to study the immense causal response of Ap-index to SFI is using the so-called superposed-epoch analysis (Kharayat et al., 2016; Pokharia et al., 2018). This is in fact similar to what we have used earlier in our PC analysis in Section 3 and in Figure 9, i.e., the superposed cycles (Takalo and Mursula, 2018; Takalo, 2021a,b, 2022a). The difference is here that we use another time series (signal) as a trigger in recording the epochs. Here we use as a zero day the timestamp when SFI exceeds some fixed level, which depends

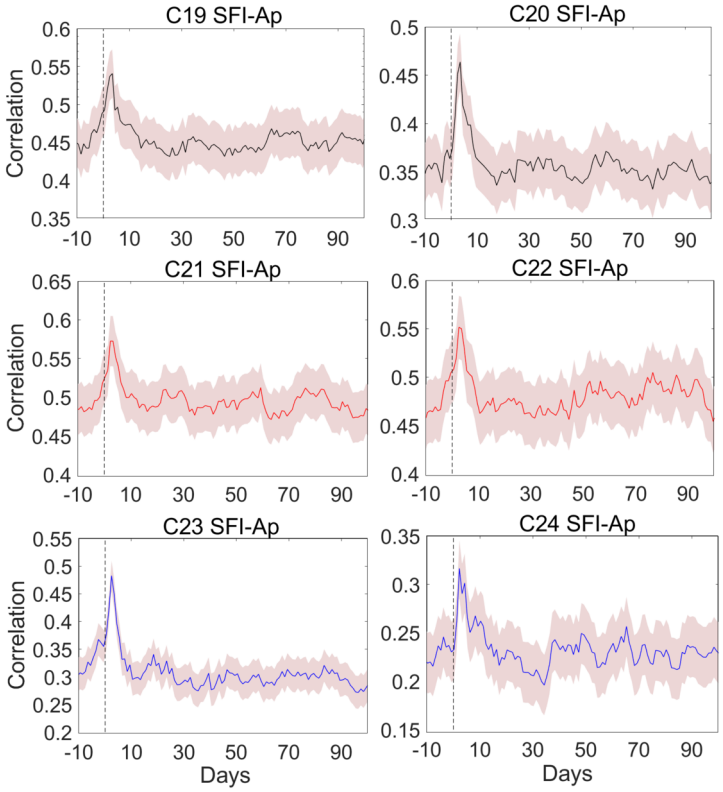

Figure 11 Magnification of the cross-correlations between SFI and Ap-index for Solar Cycles 18 – 24. The lilac color in the background shows two standard deviation limits.

on the activity of the cycle. We choose the level such that one cycle includes 10–25 epochs. Figure 12 shows the superposed epoch analysis for Solar Cycles 19 – 24. The zero day shows the average SFI (red), which has triggered the recording, and blue curve shows the response of the Ap-index to the SFI. Note that Ap maximizes 2–3 days after the triggering peak in SFI. It is evident that the results are similar to the cross-correlation analysis. We show here the time interval $-30-50$ days, i.e., start recording 30 days before the zero day. The inserted text in the figures shows the SFI triggering level and the number of superposed epochs in each cycle. Note that Cycles 19 and 20 differ from others so that there are two peaks after the peak in SFI. This is probably related to the knee in the peaks of Cycles 19 and 20 in Figure 11. Furthermore, Cycle 24 has a twofold peak similarly to that in the cross-correlation of Cycle 24 in Figure 11.

6. Comparison of SFI Cycles

Figure 13 shows the different categories of the number of SFI days for Solar Cycles 18 – 24. The figure is cumulative such that the cyan color shows all days with SFI > 0, blue color SFI > 5, red color SFI > 15, and white color SFI > 25. Everything under the y-axis value 30 and above the cyan color area means days with no Hα solar flare. Note that saturation

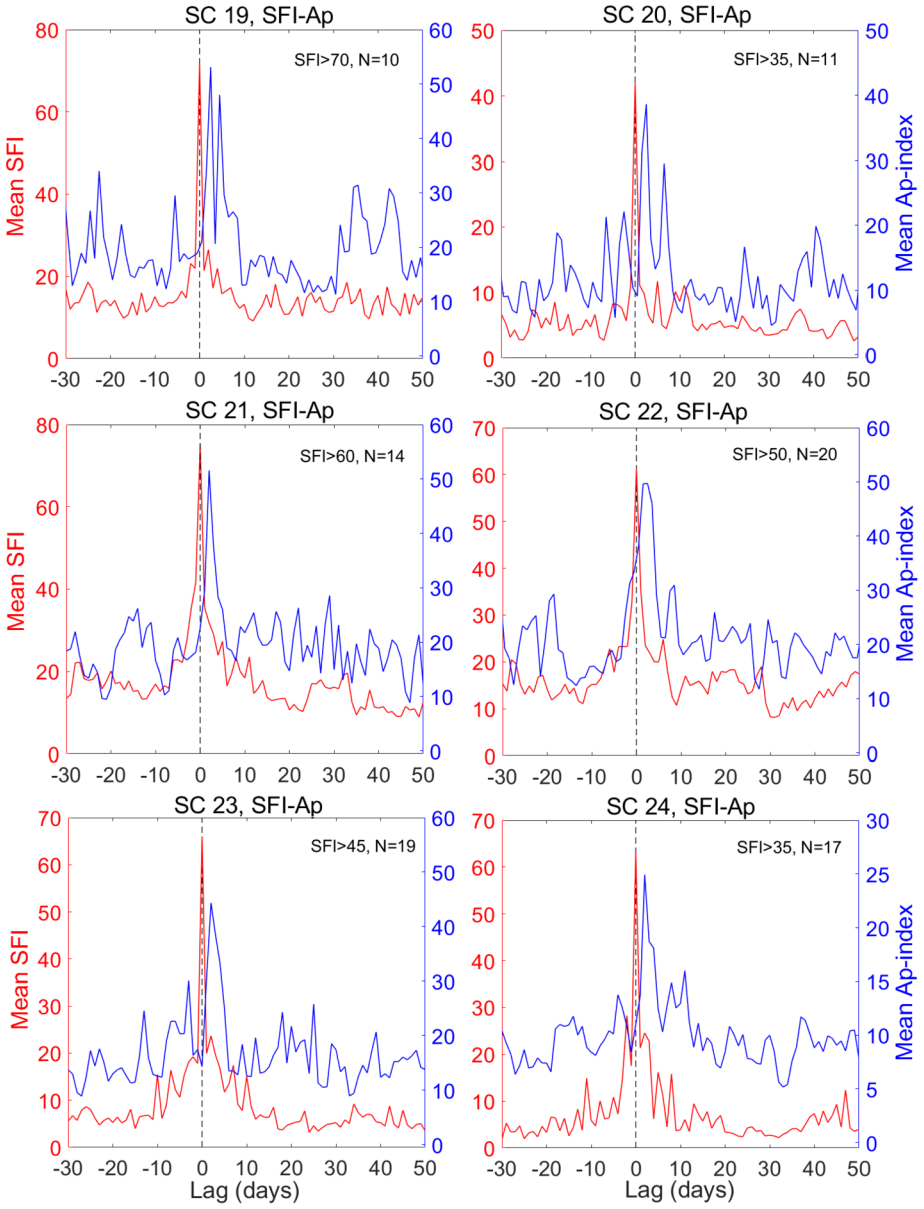

Figure 12 Superposed-epoch analysis of SFI – Ap mutual dependence for Solar Cycles 19 – 24.

level is at 30, because each point of the curves represents one month. (We have used three-month trapezoidal smoothing to make the figure more readable, and the small lumps on top of the saturation level of the cyan curve are due to months that have 31 days.) The minima between the cycles are shown as dashed black vertical lines, and the maxima of the cycles with magenta vertical lines.

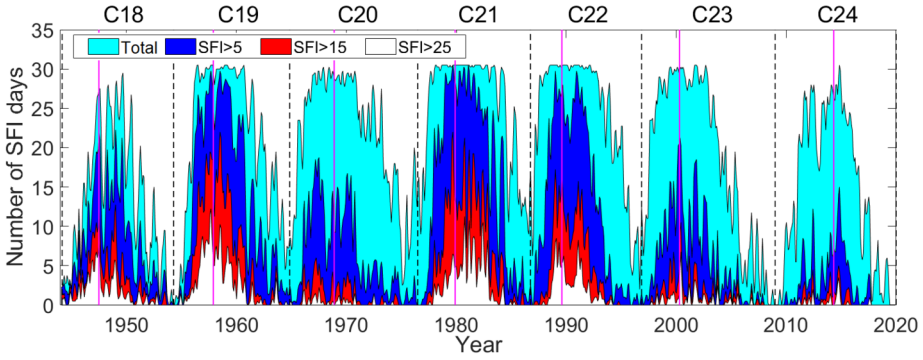

Figure 13 Number of SFI days as cumulative categories for Solar Cycles 18 – 24.

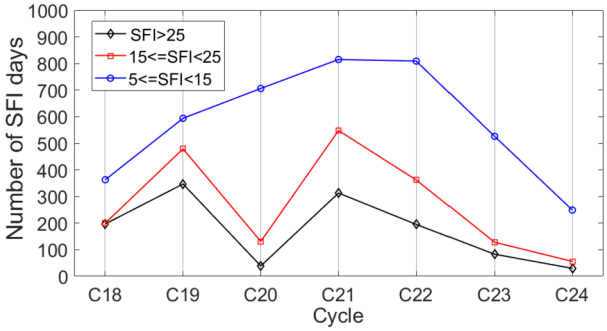

Figure 14 Number of SFI days for moderate ($5 < SFI \leq 15$), strong ($15 < SFI \leq 25$), and very strong ($SFI > 25$) categories of Cycles 18 – 24.

Figure 14 shows the different categories of the solar flare days for Solar Cycles 18 – 24 in a different way, i.e., as the total numbers of different categories, moderate ($5 \leq SFI < 15$), strong ($15 \leq SFI < 25$), and very strong ($SFI > 25$) SFI days. Cycles 19, 21, and 22 seem to have Hα flares almost every day, except at the beginning and end of the cycle (Figure 13), but Cycles 19 and 21 have by far most strong and very strong category SFI days. Note that Cycles 19, 21, and 22 have also the strongest overall cross-correlations between SFI and Ap-index in Figure 10. The longest Cycles 20 and 23 are very similar in the overall distribution, and they have about the same amount of strong SFI days. Their difference is that Cycle 20 has much more moderate SFI days and much less very strong SFI days compared to Cycle 23. As expected, Cycle 24 is the weakest cycle in every respect, although it has 30 very strong SFI days comparable to 39 very strong days of Cycle 20. Cycle 18 is somewhat a mystery, because it has so few moderate SFI days, quite a lot very strong SFI days, but lower total number of SFI days than Cycle 24 (SFI days for Cycles 18 and 24 are 1660 and 1940, respectively). There is, instead, a (quasi)annual variation in the total number of SFI days. We believe that some weak SFI days were missed in Cycle 18 flare investigation. The SFI also obeys the so-called Gnevyshev–Ohl rule for the even–odd cycle pairs, i.e., that an even cycle is weaker than the following odd cycle. This is true in SFI for cycle pairs 18–19 and 20–21 but not anymore for the cycle pair 22–23. It is, however, known that there are violations and some controversy about the G-O rule (Tlatov, 2013; Zolotova and Ponyavin, 2015).

Cycle 20 is interesting. It has the second largest amount of SFI days (3036), and only Cycle 21 has more, i.e., 3124 SFI days. It is, however, interesting that there are only 39

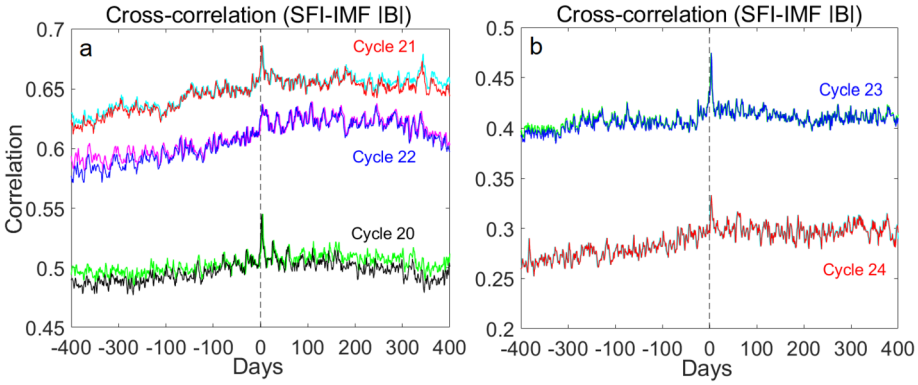

Figure 15 The cross-correlations between SFI and IMF $|B|$-component: a) for Cycles 20 – 22 and b) for Cycles 22 and 23.

very strong days in Cycle 20. We should remember that Cycle 20 was the era for the Apollo missions. We were lucky that the Apollo missions were carried out during the maximum and descending phase of Cycle 20, which was much less active than the preceding grand maximum Cycle 19 and the succeeding Cycle 21. None of the Apollo flights encountered solar flares with powerful radiation or energetic particles. The only flight with quite strong Hα flares was the Apollo mission 12; other flights were carried out during the periods of only weak flare events, except mission 13, which had some moderate activity days. According to our calculations, the preparatory flights 8 – 10 were done during the GG period of Cycle 20. However, because extreme events are unpredictable, one of the most energetic and fastest solar flare events erupted on 4 August 1972, but again luckily between the last flights Apollo 16 and 17. On the other hand, minimum of the cosmic-rays was not as deep for Cycle 20 as for Cycles 19 and 21, and the recovery phase started quite early in the descending phase of this cycle, allowing more cosmic rays enter to the vicinity of the Earth during Apollo missions (Takalo, 2022a).

7. Conclusions

We have shown that the solar flare index shows a distinct Gnevyshev gap for Solar Cycles 18 – 24. This is especially deep for the even cycles. This gap is very clear already in its PC1, which usually presents the most relevant features of the time series in question. It seems that the gap is distinctive for strong ($15 < \text{SFI} \leq 25$) and very strong ($\text{SFI} > 25$) category SFI days for the even cycles. For the odd cycles, the gap is seen already in the moderate ($5 < \text{SFI} \leq 15$) category SFI days but is not as clear as in the even cycles for the strong and very strong category SFI days.

We also show that the gap is seen in the IMF Bv^2-component at the distance of the Earth and in geomagnetic Ap-index about half a year later as a deep decline. The immediate influence of the flares is seen after two to three days as a huge peak in the cross-correlation of the SFI and Ap-index. We confirm the response of the Ap-index using superposed-epoch analysis. Furthermore, the peak exists also in the cross-correlation function of the SFI and IMF $|B|$-component. Figure 15 shows the cross-correlations between SFI and IMF $|B|$ for Solar Cycles 20 – 24. There are clear peaks at two to three days (SFI preceding IMF) for all

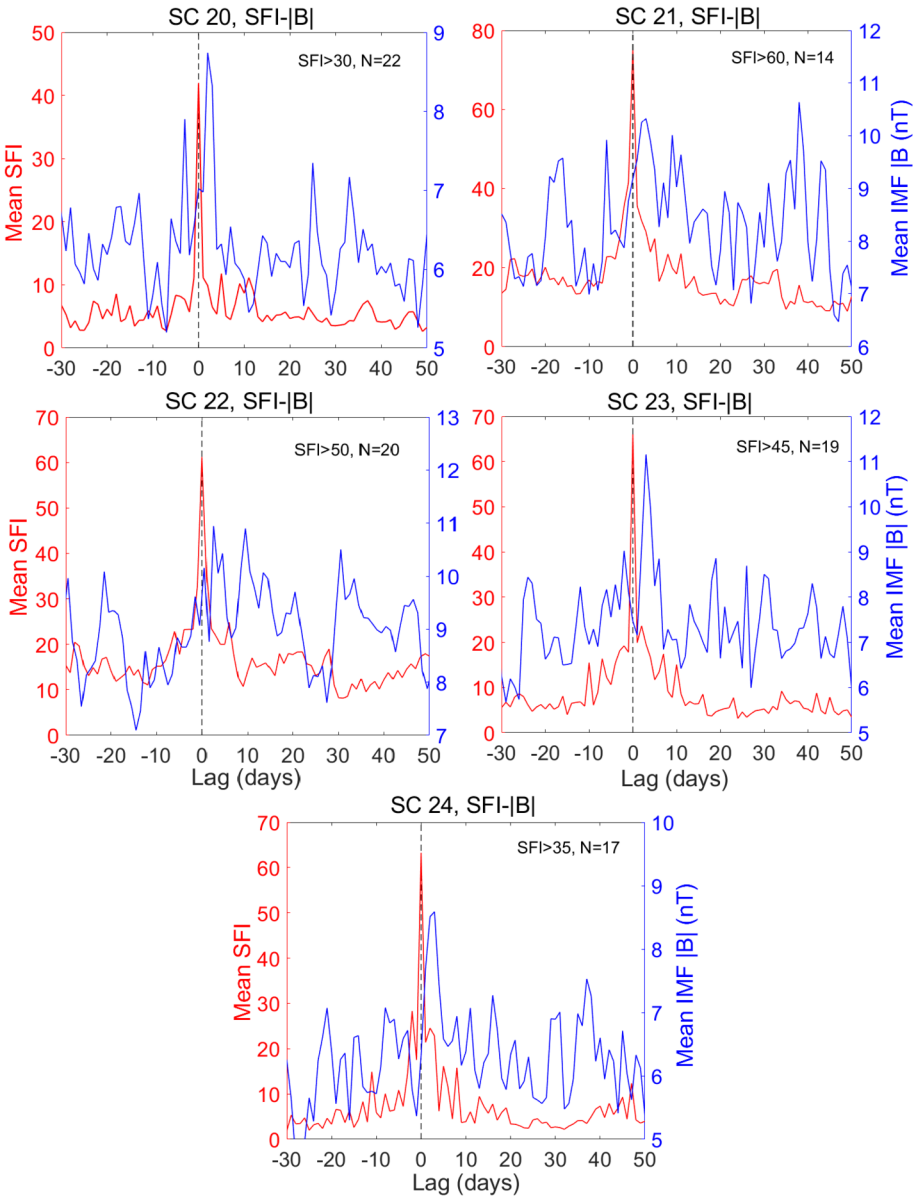

Figure 16 Superposed-epoch analysis of SFI – IMF $|B|$-component mutual dependence for Solar Cycles 20 – 24.

cycles, except Cycle 22, which has only a small enhancement. The peaks are smaller than in the cross-correlation between SFI and Ap (see Figure 10). It is evident that the correlation levels are in the same order as the activity levels of the SFI cycles. The colors and methods used here are similar to those used earlier in Figure 10. Note that the two calculated cross-correlations differ somewhat further away from the zero point but are very similar at the region of the cross-correlation peak.

We also do similar superposed-epoch analysis for the SFI – IMF $|B|$ mutual dependence to confirm the aforementioned result. Figure 16 shows this analysis for Solar Cycles 20 – 24. Note that the response of the IMF $|B|$ after two to three days is very clear, except for Cycles 21 and 22. This is because of the high overall level of the IMF $|B|$ in these active cycles. The inserted text tells again the SFI triggering level and the number of superposed epochs in each cycle.

The odd Cycles 19 and 21 are most active as measured with the average daily strength of SFI, i.e., 8.63 and 9.29, respectively. From the even cycles, the Cycle 22 has the highest activity in numbers of SFI days and also in the average daily value, i.e. 2917 SFI days and an average SFI 6.99. Cycle 18 has the same amount of very strong SFI days than Cycle 22, but interestingly least nonzero SFI days from all Cycles 18 – 24. We believe that something has happened in the recording of the smallest Hα flares between Cycles 18 and 19, and there should be more nonzero SFI days in Cycle 18. We have not analyzed Cycle 17 earlier in this study, because recording started 1937, and Cycle 17 is incomplete. However, it seems that Cycle 17 has relatively the same amount of nonzero SFI days as Cycle 18, although it is more active in flares than Cycle 18, i.e., the average SFI days are 8.37 and 5.36 for the Cycles 17 and 18, respectively. Notice that in this respect, Cycle 17 is almost as active as Cycles 19 and 21 (Velasco Herrera et al., 2022). This is in line with our aforementioned impression. Cycles 20, 23, and 24 are, however, the weakest flare cycles in this study, and their average SFI days are 3.30, 3.17, and 2.30, respectively.

In a detailed daily study, it seemed that the GGs are more or less simultaneous in all photospheric and chromospheric indices for the even cycles. Only corona index (CI) has its GG later and somewhat shallower than for the other solar parameters. For the odd cycles the GG in SFI is somewhat earlier and less deep than the GG for the even cycles. For the odd cycles GG of the other indices, except PA, lag the SFI about one solar rotation period. On the other hand, the GG in PA for the odd cycles starts much later, i.e., similarly to the GG for the even cycles about 1380 days after preceding minimum of the cycle.

The GG is in solar indices, especially in the SFI, so clear that it must have influence on the space-weather as suggested earlier by Storini et al. (2003). If we can predict the forthcoming length of the solar cycle, then it is possible to foresee the less active (GG-related) time interval in the solar-terrestrial interaction.

Acknowledgments The Solar Flare index data were obtained from https://dataverse.harvard.edu/dataset.xhtml?persistentId=doi:10.7910/DVN/U5GR3D. Part of the Flare Index Data used were calculated by T. Atac and A. Ozguc from Bogazici University Kandilli Observatory, Istanbul, Turkey. The dates of cycle minima were obtained from the National Geophysical Data Center, Boulder, Colorado, USA (https://www.ngdc.noaa.gov/stp/space-weather/solar-data/solar-indices/sunspot-numbers/cycle-data/table_cycle-dates_maximum-minimum.txt). The newly reconstructed corona indices were obtained from www.ngdc.noaa.gov/stp/solar/corona.html. The corona index for Solar Cycle 24 was downloaded from www.suh.sk/obs/vysl/MCI.htm. The SSN2 data has been downloaded from www.sidc.be/silso/datafiles, and the solar radio flux data from lasp.colorado.edu/lisird/data/penticton_radio_flux/. Definitive values of Ap are provided by GeoForschungs Zentrum (GFZ) Potsdam. The OMNI2 data are downloaded from https://spdf.gsfc.nasa.gov/pub/data/omni/low_res_omni/. Daily plage area data are from http://cdsarc.u-strasbg.fr/ftp/J/A+A/639/A88/comp_d.dat.

Author contributions All analyses, figures and writing done by the author. None other has reviewed the manuscript.

Funding Note Open Access funding provided by University of Oulu including Oulu University Hospital.

Declarations

Competing interests The authors declare no competing interests.

References

Ahluwalia, H.S.: 2000, Ap time variations and interplanetary magnetic field intensity. *J. Geophys. Res.* **105**, 27481. DOI.

Ahluwalia, H.S., Kamide, Y.: 2004, Gnevyshev gap, Forbush decrease, ICME/SSC, and Solar wind. In: Paillé, J.-P. (ed.) *35th COSPAR Scientific Assemb*, 470. ADS.

Ataç, T., Özgüç, A.: 2006, Overview of the solar activity during solar Cycle 23. *Solar Phys.* **233**, 139. DOI. ADS.

Bazilevskaya, G.A., Makhmutov, V.S., Sladkova, A.I.: 2006, Gnevyshev gap effects in solar energetic particle activity. *Adv. Space Res.* **38**, 484. DOI.

Bhattacharyya, A., Okpala, K.C.: 2015, Principal components of quiet time temporal variability of equatorial and low-latitude geomagnetic fields. *J. Geophys. Res.* **120**, 8799. DOI.

Box, G.E.P., Jenkins, G.M., Reinsel, G.C., Ljung, G.M.: 2016, *Time Series Analysis: Forecasting and Control*, 5th edn. Wiley, New York.

Bro, R., Smilde, A.K.: 2014, Principal component analysis. *Anal. Methods* **6**, 2812.

Cliver, E.W., Schrijver, C.J., Shibata, K., Usoskin, I.G.: 2022, Extreme solar events. *Living Rev. Solar Phys.* **19**, 2. DOI. ADS.

Derrick, B., Deirdre, T., White, P.: 2016, Why Welch's test is Type I error robust. *Quant. Meth. Psychol.* **12**, 30. http://eprints.uwe.ac.uk/27232.

Du, Z.L.: 2015, Bimodal structure of the solar cycle. *Astrophys. J.* **804**, 15. DOI. ADS.

Gnevyshev, M.N.: 1963, The corona and the 11-year cycle of solar activity. *Soviet Astron.* **7**, 311.

Gnevyshev, M.N.: 1967, On the 11-years cycle of solar activity. *Solar Phys.* **1**, 107. DOI. ADS.

Gnevyshev, M.N.: 1977, Essential features of the 11-year solar cycle. *Solar Phys.* **51**, 175. DOI. ADS.

Hannachi, A., Jolliffe, I.T., Stephenson, D.B.: 2007, Empirical orthogonal functions and related techniques in atmospheric science: a review. *Int. J. Climatol.* **27**, 1119. DOI.

Holappa, L., Mursula, K., Asikainen, T.: 2014, A new method to estimate annual solar wind parameters and contributions of different solar wind structures to geomagnetic activity. *J. Geophys. Res.* **119**, 9407. DOI. ADS.

Holappa, L., Mursula, K., Asikainen, T., Richardson, I.G.: 2014, Annual fractions of high-speed streams from principal component analysis of local geomagnetic activity. *J. Geophys. Res.* **119**, 4544. DOI. ADS.

Kharayat, H., Prasad, L., Mathpal, R., Garia, S., Bhatt, B.: 2016, Study of cosmic ray intensity in relation to the interplanetary magnetic field and geomagnetic storms for Solar Cycle 23. *Solar Phys.* **291**, 603. DOI.

Kleczek, J.: 1952, Ionospheric disturbances and flares in the 11-years cycle. *Bull. Astron. Inst. Czechoslov.* **3**, 52.

Knoska, S.: 1985, Distribution of flare activity on the solar disk in the years 1937–1976. *Contrib. Astron. Obs. Skaln. Pleso* **13**, 217. ADS.

Knoška, S., Petrašek, J.: 1984, Chromospheric flare activity in SOLAR-CYCLE-20. *Contrib. Astron. Obs. Skaln. Pleso* **12**, 165.

Krishnamoorthy, K.: 2006, *Handbook of Statistical Distributions with Applications*, Chapman & Hall/CRC, Taylor & Francis Group, Boca Raton, 128. ISBN 1-58488-635-8.

Kumar, D., Rai, C.S., Kumar, S.: 2008, Principal component analysis for data compression and face recognition. *INFOCOMP J. Comput. Sci.* **7**, 48.

Li, C., Fei, Y., Tian, X.A., An, J.M.: 2021, The midrange periodicities of solar Hα flare index during Solar Cycles 21–24. *Astrophys. Space Sci.* **366**, 65. DOI. ADS.

Lin, J.-W.: 2012, Ionospheric total electron content seismo-perturbation after Japan's March 11, 2011, $M = 9.0$ Tohoku earthquake under a geomagnetic storm; a nonlinear principal component analysis. *Astrophys. Space Sci.* **341**, 251. DOI.

Lou, Y.-Q.: 2000, Rossby-type wave-induced periodicities in flare activities and sunspot areas or groups during solar maxima. *Astrophys. J.* **540**, 1102. DOI. ADS.

Mendoza, B., Velasco-Herrera, V.: 2011, On mid-term periodicities in sunspot groups and flare index. *Solar Phys.* **271**, 169. DOI. ADS.
Nagovitsyn, Y.A., Ivanov, V.G., Osipova, A.A.: 2019, Features of the Gnevyshev–Waldmeier rule for various lifetimes and areas of sunspot groups. *Astron. Lett.* **45**, 695. DOI. ADS.
Norton, A.A., Gallagher, J.C.: 2010, Solar-cycle characteristics examined in separate hemispheres: phase, Gnevyshev gap, and length of minimum. *Solar Phys.* **261**, 193. DOI. ADS.
Okpala, K., Okeke, F.: 2014, Variability of the daily cosmic ray count rates in the northern hemisphere. In: Willis, P. (ed.) *40th COSPAR Sci. Ass.* **40**, D1.3.
Oloketuyi, J., Liu, Y., Zhao, M.: 2019, The periodic and temporal behaviors of solar X-ray flares in Solar Cycles 23 and 24. *Astrophys. J.* **874**, 20. DOI. ADS.
Özgüç, A., Ataç, T.: 1989, Periodic behaviour of solar flare index during SOLAR-CYCLE-20 and SOLAR-CYCLE-21. *Solar Phys.* **123**, 357. DOI. ADS.
Özgüç, A., Ataç, T., Rybák, J.: 2002, Short-term periodicities in the flare index between the years 1966-2001. In: Wilson, A. (ed.) *Solar Variability as an Input to the Earth's Environment*, *ESA Special Publication* **535**, 141. ADS.
Özgüç, A., Ataç, T., Rybák, J.: 2003, Temporal variability of the flare index (1966–2001). *Solar Phys.* **214**, 375. DOI. ADS.
Özgüç, A., Kilcik, A., Sarp, V., Yeşilyaprak, H., Pektaş, R.: 2021, Periodic variation of solar flare index for the last solar cycle (Cycle 24). *Adv. Astron.* **2021**, 5391091. DOI. ADS.
Pokharia, M., Prasad, L., Bhoj, C., Mathpal, C.: 2018, Study of geomagnetic storms and solar and interplanetary parameters for Solar Cycles 22 and 24. *Solar Phys.* **293**, 126. DOI.
Richardson, I.G., Cane, H.V.: 2005, The 150 day quasi-periodicity in interplanetary and solar phenomena during Cycle 23. *Geophys. Res. Lett.* **32**, L02104. DOI. ADS.
Rieger, E., Share, G., Forrest, D.J., Kanbach, G., Reppin, C., Chupp, E.L.: 1984, A 154-day periodicity in the occurrence of hard solar flares? *Nature* **312**, 623. DOI.
Schove, D.J.: 1979, Sunspot turning-points and aurorae since A.D. 1510. *Solar Phys.* **63**, 423. DOI. ADS.
Snedecor, G.W., Cochran, W.G.: 1989, *Statistical Methods*, 8th edn. Iowa State University Press, Ames, 64. ISBN 978-0-8138-1561-9.
Storini, M., Bazilevskaya, G.A., Fluckiger, E.O., Krainev, M.B., Makhmutov, V.S., Sladkova, A.I.: 2003, The Gnevyshev gap: a review for space weather. *Adv. Space Res.* **31**, 895. DOI.
Suresh, K., Gopalswamy, N., Shanmugaraju, A.: 2022, Arrival time estimates of Earth-directed CME-driven shocks. *Solar Phys.* **297**, 3. DOI.
Švestka, Z.: 1956, Several notes on the statistics of chromospheric flares. *Bull. Astron. Inst. Czechoslov.* **7**, 9. ADS.
Takalo, J.: 2020a, Comparison of latitude distribution and evolution of even and odd sunspot cycles. *Solar Phys.* **295**, 49. DOI.
Takalo, J.: 2020b, Temporal distribution of solar cycle 24 sunspot groups: comparison to Cycles 12-23. *Ann. Geophys.* **63**, DM107. DOI.
Takalo, J.: 2021a, Comparison of geomagnetic indices during even and odd Solar Cycles SC17-SC24: signatures of gnevyshev gap in geomagnetic activity. *Solar Phys.* **296**, 19. DOI.
Takalo, J.: 2021b, Separating the aa-index into solar and hale cycle related components using principal component analysis. *Solar Phys.* **296**, 80. DOI.
Takalo, J.: 2022a, Extracting hale cycle related components from cosmic-ray data using principal component analysis. *Solar Phys.* **297**, 113. DOI. ADS.
Takalo, J.: 2022b, Spatial and temporal distribution of solar green-line corona for Solar Cycles 18 – 24. *Solar Phys.* **297**, 118. DOI.
Takalo, J., Mursula, K.: 2018, Principal component analysis of sunspot cycle shape. *Astron. Astrophys.* **620**, A100. DOI.
Tlatov, A.G.: 2013, Reversals of Gnevyshev–Ohl rule. *Astrophys. J. Lett.* **772**, L30. DOI. ADS.
Torrence, C., Compo, G.P.: 1998, A practical guide to wavelet analysis. *Bull. Am. Meteorol. Soc.* **79**, 61. DOI. ADS.
Velasco Herrera, V.M., Soon, W., Knoška, Š., Perez-Peraza, J.A., Cionco, R.G., Kudryavtsev, S.M., Qiu, S., Connolly, R., Connolly, M., Švanda, M., Acosta Jara, J., Gregori, G.P.: 2022, The new composite solar flare index from Solar Cycle 17 to Cycle 24 (1937–2020). *Solar Phys.* **297**, 108. DOI.
Zharkova, V.V., Shepherd, S.J., Popova, E., Zharkov, S.I.: 2015, Heartbeat of the sun from principal component analysis and prediction of solar activity on a millennium timescale. *Nature Sci. Rep.* **5**, 15689. DOI. ADS.
Zolotova, N.V., Ponyavin, D.I.: 2015, The Gnevyshev–Ohl rule and its violations. *Geomagn. Aeron.* **55**, 902.